Electronic Supplementary Material (ESI) for Materials Horizons.
This journal is © The Royal Society of Chemistry 2021

*Supporting Information*

# Red-to-NIR Emissive Radical Cations Derived from Simple Pyrroles

Lihua Zheng,[‡a] Wenchao Zhu,[‡a] Zikai Zhou,[‡a] Kai Liu,*[b] Meng Gao,*[a] and Ben Zhong Tang*[c]

[a]National Engineering Research Center for Tissue Restoration and Reconstruction, Key Laboratory of Biomedical Engineering of Guangdong Province, Key Laboratory of Biomedical Materials and Engineering of the Ministry of Education, Innovation Center for Tissue Restoration and Reconstruction, School of Biomedical Science and Engineering, School of Materials Science and Engineering, South China University of Technology, Guangzhou 510006, China

[b]Institute of Marine Drugs, Guangxi University of Chinese Medicine, Nanning 530200, China

[c]AIE institute, State Key Laboratory of Luminescent Materials and Devices, Center for Aggregation-Induced Emission, Guangdong Provincial Key Laboratory of Luminescence from Molecular Aggregates, Guangzhou International Campus, South China University of Technology, Guangzhou 510640; Department of Chemistry, Hong Kong Branch of Chinese National Engineering Research Center for Tissue Restoration and Reconstruction and Institute for Advanced Study, The Hong Kong University of Science and Technology, Kowloon, Hong Kong 999077; Shenzhen Institute of Aggregate Science and Technology, School of Science and Engineering, The Chinese University of Hong Kong, Shenzhen 518172, China

[‡] These authors contributed equally to this work.

**Table of Contents**


Materials and chemicals 2
Equipment and methods 2
Synthesis and characterization of pyrroles 3
Excitation and emission spectra measurement of pyrrole derived radical cations on TLC plate 4
Synthesis and characterization of **P6**$^{\bullet+}$⊂CB[7] complex 4
Cyclic voltammetry measurement 5
EPR measurement 5
EPR calculation 5
Fluorescence quantum yield and lifetime measurement 5
Theoretical calculation of **P6**$^{\bullet+}$ and **P6**$^{\bullet+}$⊂CB[7] 5
Cell culture 6
Cell viability measurement 6
Cell imaging 6
In vivo imaging 7
**Table S1**. Photophysical properties of pyrrole derived radical cations 8
**Tabel S2**. Electrochemical properties of **P1-P10** 8
**Figure S1**. $^{1}$H NMR spectrum of **P1** 9
**Figure S2**. $^{1}$H NMR spectrum of **P3** 9
**Figure S3**. $^{1}$H NMR spectrum of **P4** 10
**Figure S4**. $^{1}$H and $^{13}$C NMR spectrum of **P6** 11
**Figure S5**. $^{1}$H NMR spectrum of **P7** 12
**Figure S6**. $^{1}$H NMR spectrum of **P8** 12
**Figure S7**. PL spectra of **P1**$^{\bullet+}$ on TLC plate under dark and relative PL intensities changes 13
**Figure S8**. Normalized PL spectra of **P1**$^{\bullet+}$ with different excitation wavelengths 14
**Figure S9**. PL spectra and photos of **P1**$^{\bullet+}$ on TLC plate under air and argon 15
**Figure S10.** Fluorescence lifetime spectra of **P1**$^{\bullet+}$, **P6**$^{\bullet+}$, **P7**$^{\bullet+}$, **P8**$^{\bullet+}$, **P9**$^{\bullet+}$ and **P6**$^{\bullet+}$⊂CB[7] 14
**Figure S11**. PL spectra and intensity changes of **P2**$^{\bullet+}$, **P3**$^{\bullet+}$, **P4**$^{\bullet+}$, **P5**$^{\bullet+}$, **P10**$^{\bullet+}$ on TLC plate 15
**Figure S12**. Normalized excitation spectra of pyrrole radical cations on TLC plate 15
**Figure S13**. EPR spectra of **P1**$^{\bullet+}$, **P7**$^{\bullet+}$, **P8**$^{\bullet+}$, **P9**$^{\bullet+}$, **P10**$^{\bullet+}$ and **P6**$^{\bullet+}$⊂CB[7] 16
**Figure S14**. Oxidative and reductive cyclic voltammograms of **P1-P10** 16
**Figure S15**. Time-dependent PL and excitation spectra of **P6**$^{\bullet+}$ on TLC plate 17
**Figure S16**. UV-Vis absorption and PL spectra of **P6**$^{\bullet+}$⊂CB[7] with different molar ratio 17
**Figure S17**. The ITC titration curve for **P6**$^{\bullet+}$⊂CB[7] 18
**Figure S18**. Time-dependent UV-Vis absorption and PL spectra of **P6**$^{\bullet+}$⊂CB[7] 18
**Figure S19**. Mulliken spin population analysis of **P6**$^{\bullet+}$⊂CB[7] 19
**Figure S20**. Cell viabilities of HeLa and A375 cells incubated with **P6**$^{\bullet+}$⊂CB[7] 19
**Figure S21**. The intensity profile of ROI lines in cell imaging 19
**Figure S22**. Photostability of **P6**$^{\bullet+}$⊂CB[7] in HeLa cells 20
**Figure S23**. CLSM images of HeLa cells treated with **P6**$^{\bullet+}$⊂CB[7] and GSH/ascorbic acid 20
**Figure S24**. Cell images of **P6**$^{\bullet+}$⊂CB[7] without and with pre-treatment of CCCP 20
**Figure S25**. Cell images and in situ fluorescence spectra of **P6**$^{\bullet+}$⊂CB[7] 21

## Materials and chemicals

Compounds **P1**, **P3**, **P4**, **P6**, **P7**, **P8** were prepared according to a literature method.[1-2] Compounds **P2**, **P10**, aniline, *p*-anisidine, 4-aminobenzoic acid and acetonylacetone were purchased from Macklin (Shanghai, China); Compound **P5** was purchased from Bide Pharmatech Ltd.; Compound **P9** and 1,4-diphenyl-1,4-butanedione were purchased from TCI Chemical Co.; 1-phenylpentane-1,4-dione were purchased from Alfa Aesar; Sodium borohydride ($NaBH_4$) and iodine were purchased from Aladdin. Tetrahydrofuran (THF) and methanol (MeOH) were purchased from Tianjin Chemical Reagent Factory. Other solvents were purchased from Energy Chemical and directly used without further purification. MitoTracker Green was purchased from Beyotime Biotechnology. Cucurbit[7]uril (CB[7]) was purchased fron ShangHai SuperLan Chemical Tech Centre. Dulbecco's Modified Essential Medium (DMEM), fetal bovine serum (FBS) and Phosphate buffered saline (PBS) were purchased from Gibco (Life Technologies). Ultra-pure water was supplied by Milli-Q Plus System (Millipore Corporation, United States).

## Equipment and methods

The UV-Vis absorption spectra were measured on a Shimadzu UV-2600 spectrophotometer, medium scanning rate, and quartz cuvettes of 1 cm path length. The photoluminescence spectra for solution samples were measured on a Fluorescence Spectrophotometer F-7000. The photoluminescence spectra for solid samples were measured on a microplate reader (Tecan Infinite M200 PRO). The Electron-Paramagnetic Resonance (EPR) spectra were measured on a Bruker E500-10/12 Electron-Paramagnetic Resonance CW. ITC experiment was performed on a MicroCal system, VP-ITC model. The absolute fluorescence quantum yield was measured on a FLS1000 fluorescence spectrophotometer (Edinburgh Instruments Ltd, U.K). The fluorescence lifetime was measured on a Hamamatsu Compact Fluorescence Lifetime Spectrometer C11367. The $^{1}H$ and $^{13}C$ NMR spectra were measured on a Bruker AV 400 or 600 NMR spectrometer. Confocal lasing scanning microscopic (CLSM) images were obtained on the confocal microscope (Zeiss Laser Scanning Confocal Microscope; LSM880). Automated cell counter (Countess

II) was employed for cell counting. The cell viability assay was conducted on a microplate reader (Tecan Infinite M200 PRO). The in vivo whole body and ex vivo organ fluorescence images were taken on Xenogen IVIS Spectrum imager (Caliper Life Sciences Inc., USA).

**Synthesis and characterization of P6**

Compound **P5** (155.3 mg, 0.7 mmol) was first dissolved in methanol (5 mL) and $NaBH_4$ (159.5 mg, 4.2 mmol) was then added, the mixture was stirred at room temperature for 30 min. After completion of the reaction, the precipitation was filtered, washed by $H_2O$ and further dried under vacuum to yield **P6** as a light yellow solid (120 mg, 85% yield). $^1$H NMR (400 MHz, MeOD): δ 7.50 (t, *J* = 7.4 Hz, 2H), 7.38–7.35 (m, 1H), 7.25–7.06 (d, *J* = 7.2 Hz, 2H), 5.91 (s, 1H), 4.44 (s, 2H), 1.97 (s, 3H), 1.96 (s, 3H); $^{13}$C NMR (151 MHz, MeOD): δ 139.0 , 128.9 , 128.1 , 127.6, 127.3, 126.0 , 118.4 , 106.7 , 56.5 , 11.5 , 9.2. ESI-HRMS: m/z $[M + Na]^+$ calcd for $C_{13}H_{15}NNaO$: 224.1051; found: 224.1051.

**Compounds P1, P3, P4, P7, P8 were prepared according to the literature method.**[1-2]

$^1$H NMR of **P1** (400 MHz, $CDCl_3$): δ 7.45 (t, *J* = 7.6 Hz, 2H), 7.40 (t, *J* = 6.8 Hz, 1H), 7.21 (d, *J* = 8.0 Hz, 2H), 5.90 (s, 2H), 2.03 (s, 6H).

$^1$H NMR of **P3** (400 MHz, $CDCl_3$): δ 7.36 (br s, 2H), 7.25–7.22 (m, 2H), 7.18–7.12 (m, 5H), 7.08–7.01 (m, 6H), 6.48 (s, 2H).

$^1$H NMR of **P4** (600 MHz, $d_6$-DMSO): δ 7.45–7.41 (m, 2H), 7.40–7.36 (m, 1H), 7.19-7.18 (m, 2H), 7.15–7.12 (m, 2H), 7.08–7.04 (m, 1H), 7.02–6.98 (m, 2H), 6.31 (d, *J* = 3.6 Hz, 1H), 6.04 (d, *J* = 3.6 Hz, 1H), 2.05 (s, 3H).

$^1$H NMR of **P7** (600 MHz, $d_6$-DMSO): δ 7.16 (d, *J* = 9.0 Hz, 2H), 7.04 (d, *J* = 9.0 Hz, 2H), 5.76 (s, 2H), 3.81 (s, 3H), 1.93 (s, 6H).

$^1$H NMR of **P8** (400 MHz, $CDCl_3$): δ 8.23 (d, *J* = 6.0 Hz, 2H), 7.34 (d, *J* = 6.3 Hz, 2H), 5.95 (s, 2H), 2.07 (s, 6H).

**Excitation and emission spectra measurement of in situ generated pyrrole-derived radical cations on TLC plate**

20 μL of pyrrole stock solution in $CH_2Cl_2$ (100 mM) was added onto TLC plate, which was futher

irradiated under 365 nm UV lamp for different time and the exciation and emission spectra were measured on a microplate reader (Tecan Infinite M200 PRO).

**Synthesis and characterization of P6$^{\bullet+}$⊂CB[7] complex**

Compound **P6** was first dissolved in DMSO and then added into the water solution containing CB[7] under sonication or stirring to afford **P6**$^{\bullet+}$⊂CB[7] complex with molar ratio of **P6** : CB[7] = 1 : 6–3 : 1 ([**P6**] = 300 μM) and volume ratio of DMSO : $H_2O$ = 1 : 99. The generation of **P6**$^{\bullet+}$⊂CB[7] complex can be in situ monitored by UV-Vis and PL spectra measurement.

**Isothermal titration calorimetry (ITC) experiment**

ITC experiment was performed on a MicroCal system, VP-ITC model. The solution of **P6** in $H_2O$ (0.05 mM) was added to a 1.8 mL cell and the solutions of CB[7] (0.5 mM) in $H_2O$ were added by injecting successively 10 μL of titrant over 20 s (16×) with a 220 s interval between each injection. Thermodynamic information was recorded on a one-site binding model utilizing data from which the heat of dilution of the guest was subtracted.

**Cyclic voltammetry measurement**

The cyclic voltammetry (CV) measurements were performed on a CH Instruments CHI760E electrochemical analyzer with a glass carbon disc as the working electrode, a platinum wire as the counter-electrode and $Ag/Ag^+$ as the reference electrode. The redox couple ferrocenium/ ferrocene was used as the internal standard at a rate of 50 mV $s^{-1}$. Tetrabutylammonium hexafluorophosphate dissolved in anhydrous dimethyl formamide and $CH_2Cl_2$ (0.1 M) was respectively used as the electrolyte for the negative and positive scans.

**EPR spectra measurement**

Pyrroles were first dissolved in $CH_2Cl_2$ (100 mM) and then mixed with silica gel powder under stirring. $CH_2Cl_2$ was then removed under vacuum evaporation and the solid powder was then irradiated with a

hand-held UV lamp (365 nm) for different time. The solid samples were then placed in the EPR tube and the spectra were recorded within a period of 5 min.

### EPR calculation

Based on the optimized structure of **P6**$^{\bullet+}$ by Gaussian, the EPR of **P6**$^{\bullet+}$ radical was theoretically predicted by ORCA (v4.2.1) software[3] at RI-B2PLYP/def2-TZVP with RIJCOSX enhancement to accelerate the calculation and the final isotropic value of *g* was calculated to be 2.002.

### Fluorescence quantum yield and lifetime measurement

50 μL of pyrrole stock solution in $CH_2Cl_2$ (100 mM) was added onto TLC plate, which was futher irradiated under 365 nm UV lamp for different time. The samples were then measured on FLS1000 fluorescence spectrophotometer (Edinburgh Instruments Ltd, U.K) and Hamamatsu Compact Fluorescence Lifetime Spectrometer C11367.

### Theoretical calculation of P6$^{\bullet+}$ and P6$^{\bullet+}$⊂CB[7]

The geometry optimization and frequency calculation of **P6**$^{\bullet+}$ were calculated at B3LYP/def2-TZVP with empirical dispersion correction (GD3BJ) based on density functional theory (DFT) by Gaussian16 software.[3-4] Based on the optimized structures, the excitation wavelength of **P6**$^{\bullet+}$ was calculated by time-dependent DFT with UωB97XD method at def2-TZVP basis set. For all the calculation, the solvation effect was considered by the default PCM model in $CH_2Cl_2$ solvent.

The molecular dynamics simulation of **P6**⊂CB[7] complex was calculated by AMBER20 software.[5-7] The single **P6**⊂CB[7] complex was solvated in a water box filled with 1500 TIP3P molecules. Then, two rounds of minimization were performed. In the first round, the solute was restraint during the 10000 cycles of minimization. For the second minimization step, any restraint was removed. After that, a heating step was conducted. The box was gradually heated up to 300 K by Langevin method (collision frequency, *gamma_ln*=1) within 2 ns in an NVT ensemble. Finally, a 5 ns simulation in an NPT ensemble was

continued to evaluate the equilibration of the system. The trajectory shows that **P6** can be stably encapsulated by CB[7] complex during simulation.

The final snapshot of **P6**⊂CB[7] complex from simulation was subjected to the quantum calculation by Gaussian16 software. The complex without waters was further optimized by ONIOM method. The **P6** molecule was considered as high layer with PBE0/6-31G(d), while the low layer CB[7] was treated by UFF force field. Based on the optimized structure of **P6**⊂CB[7] complex, the TDDFT was performed at UωB97XD/def2-TZVP for all atoms of $\mathbf{P6}^{\bullet+}$ encapsulated in CB[7]. For comparison, a single point calculation at UωB97XD/def2-TZVP level was performed for $\mathbf{P6}^{\bullet+}$ radical only, the initial geometry of which is the same as that in **P6**⊂CB[7] complex. It should be noted that the solvation effect was simulated by PCM model of water for all quantum calculation.

**Cell Culture**

HeLa cells and A375 cells were cultured in DMEM containing 1% penicillin-streptomycin and 10% FBS at 37 °C in a humidified atmosphere with 5% $CO_2$.

**Cell Viability Measurement**

MTT assays were used to evaluate the cytotoxicity of $\mathbf{P6}^{\bullet+}$⊂CB[7] complex. The cells were seeded in a 96-well plate with a density of $1\times10^5$ cells/mL. After incubation for 24 h, the culture medium in each well was replaced by 100 μL fresh medium containing different concentrations of $\mathbf{P6}^{\bullet+}$⊂CB[7] complex (molar ratio of $\mathbf{P6}^{\bullet+}$ : CB[7] = 3:1). After 24 h incubation, the medium was removed and fresh-prepared MTT solution (0.5 mg/mL, 100 μL) was added. After incubation at 37 °C for 4 h, the MTT solution was removed, and DMSO (100 μL) was then added into each well and the plate was gently shaken for 10 min at room temperature to dissolve all the precipitates. The absorbance of sample and control wells at 570 nm were then measured by a microplate reader. Cell viability was then calculated by the ratio of the absorbance of sample wells to control cells.

**Cell imaging**

Cells were seeded in glass-bottom cell culture dishes ($1 \times 10^5$ cells/dish) and incubated for 24 h. The cells were then stained with **P6**$^{\bullet+}$⊂CB[7] complex generated by in situ mixing of **P6** (20 μM) and CB[7] (6.67 μM) and further incubation at 37 °C for 3 h, the CLSM images were taken under confocal microscope through laser irradiation at 633 nm, $\lambda_{em}$ = 643-723 nm (Laser power: 5%).

For cell imaging in the presence of CCCP, HeLa or A375 cells were pre-treated with CCCP (20 μM) for 30 min and then treated with **P6**$^{\bullet+}$⊂CB[7] complex for 3 h at 37 °C. The fluorescence images of **P6**$^{\bullet+}$⊂CB[7] complex were taken with $\lambda_{ex}$ = 633 nm and $\lambda_{em}$ = 640-750 nm (Laser power: 5%)

**In Vivo imaging**

All mice experiments were approved by Animal Center of South China University of Technology and were performed in compliance with the Regulation on the Administration of Laboratory Animals established by the State Council, the People's Republic of China. Specific male Balb/c nude mice (5 weeks) were supplied by Guangdong Medical laboratory Animal Center. A375 cells ($2\times10^6$) were subcutaneous injected into the selected positions to establish the tumor model of Balb/c nude mice. When the tumor volume reached ≈ 200 $mm^3$, 6 mg/kg of **P6**$^{\bullet+}$⊂CB[7] (molar ratio = 3: 1) was injected into tumor and the mices were used for in vivo imaging with $\lambda_{ex}$ = 608 nm and $\lambda_{em}$ = 680 nm.

**Table S1.** The photophysical properties of pyrrole derived radical cations

| Compound | $\lambda_{ex}$ [nm][c)] | $\lambda_{em}$ [nm][d)] | $\Phi_f$ [%][e)] | $\tau$ (ns)[f)] | $k_r$ [$10^7$ $s^{-1}$][g)] | $k_{nr}$ [$10^8$ $s^{-1}$][h)] |
|---|---|---|---|---|---|---|
| **P1**$^{\bullet+}$ a) | 600 | 630 | 8.54 | 1.63 | 5.21 | 5.61 |
| **P6**$^{\bullet+}$ a) | 630 | 670 | 11.32 | 2.22 | 5.09 | 3.99 |
| **P7**$^{\bullet+}$ a) | 590 | 630 | 7.22 | 1.87 | 3.85 | 4.96 |
| **P8**$^{\bullet+}$ a) | 610 | 650 | 9.59 | 1.63 | 5.52 | 5.54 |
| **P9**$^{\bullet+}$ a) | 590 | 620 | 4.86 | 2.33 | 2.01 | 4.08 |
| **P6**$^{\bullet+}$**⊂CB[7]**[b)] | 600 | 675 | 1.33 | 1.93 | 0.67 | 5.11 |

a) Pyrrole derived radical cations generated on TLC plate under 365 nm UV irradiation; b) **P6**$^{\bullet+}$⊂CB[7] was generated by mixing of **P6** and CB[7] in water with molar ratio of **P6** : CB[7] = 3:1, [**P6**] = 10 mM; c) Maximum absorption wavelength; d) Maximum emission wavelength; e) Absolute quantum yield; f) Average fluorescence lifetime; g) Radiative relaxation rate $k_r = \Phi/\tau$; h) Non-radiative relaxation rate $k_{nr} = (1-\Phi)/\tau$.

**Table S2.** Electrochemical properties of pyrroles

| Compound | $E^{ox}_{onset}$ (V)[a)] | $E^{re}_{onset}$ (V)[b)] | HOMO (eV) | LUMO (eV) |
|---|---|---|---|---|
| **P1** | 0.67 | -2.73 | -5.18 | -2.00 |
| **P2** | 1.15 | -2.70 | -5.70 | -2.03 |
| **P3** | 0.73 | -2.66 | -5.23 | -2.07 |
| **P4** | 0.66 | -2.68 | -5.24 | -2.05 |
| **P5** | 1.02 | -2.41 | -5.58 | -2.15 |
| **P6** | 0.62 | -1.65 | -5.19 | -3.07 |
| **P7** | 0.64 | -2.64 | -5.21 | -2.08 |
| **P8** | 0.73 | -2.30 | -5.30 | -2.42 |
| **P9** | 0.53 | -2.66 | -5.09 | -2.06 |
| **P10** | 0.50 | -2.69 | -5.05 | -2.04 |

a) Oxidation potentials; b) Reduction potentials.

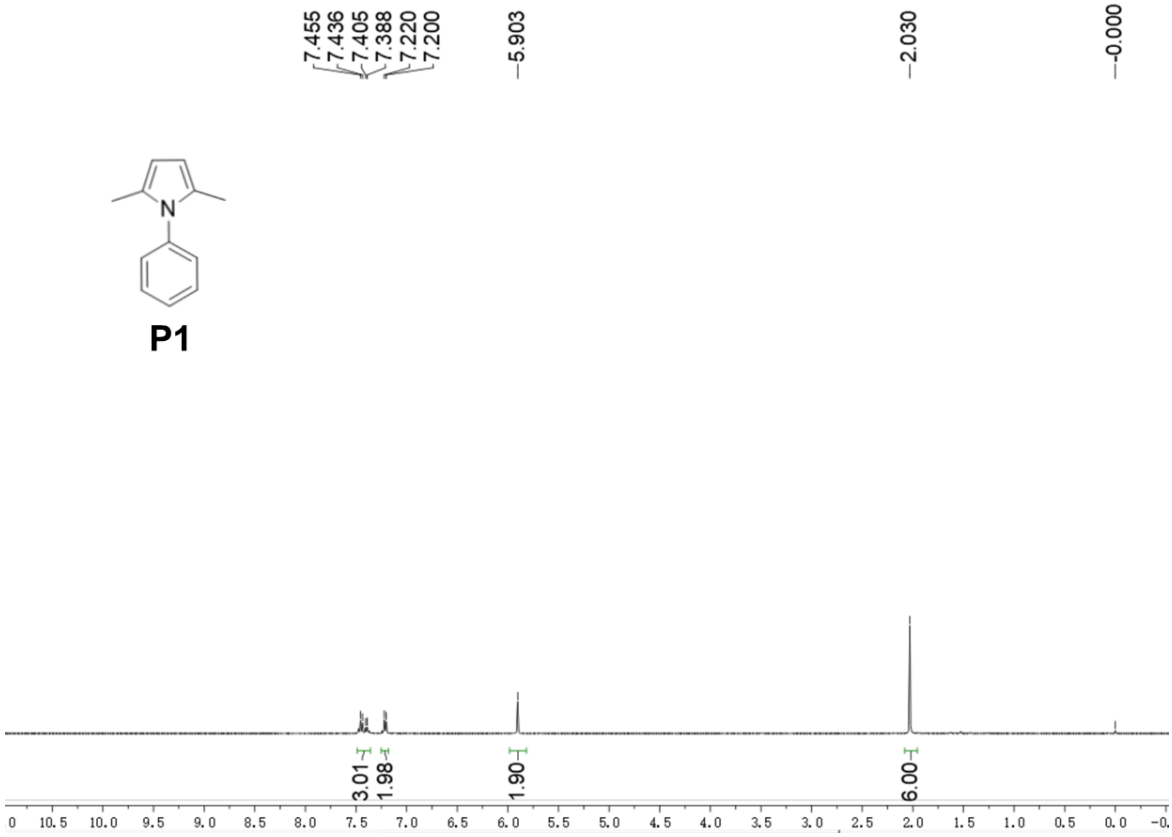


**Figure S1.** $^{1}$H NMR spectrum of **P1** in $CDCl_3$.

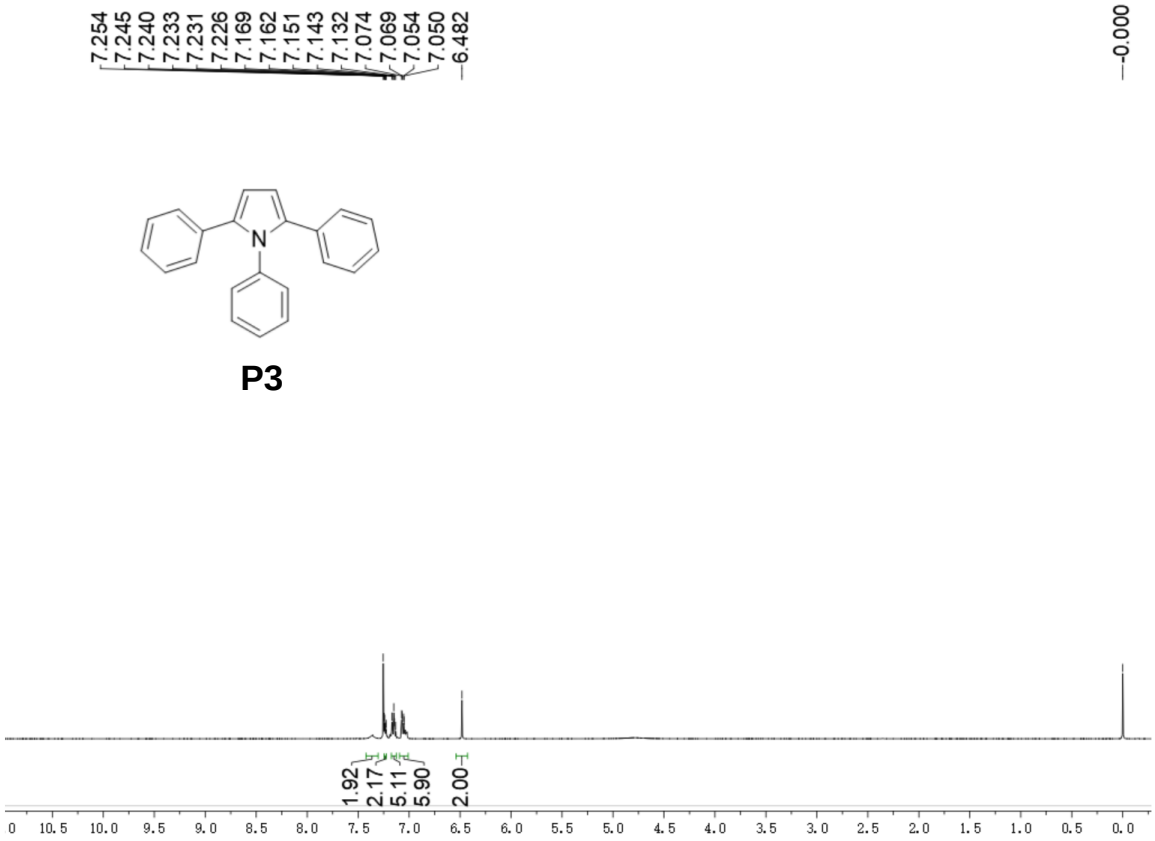


**Figure S2.** $^{1}$H NMR spectrum of **P3** in $CDCl_3$.

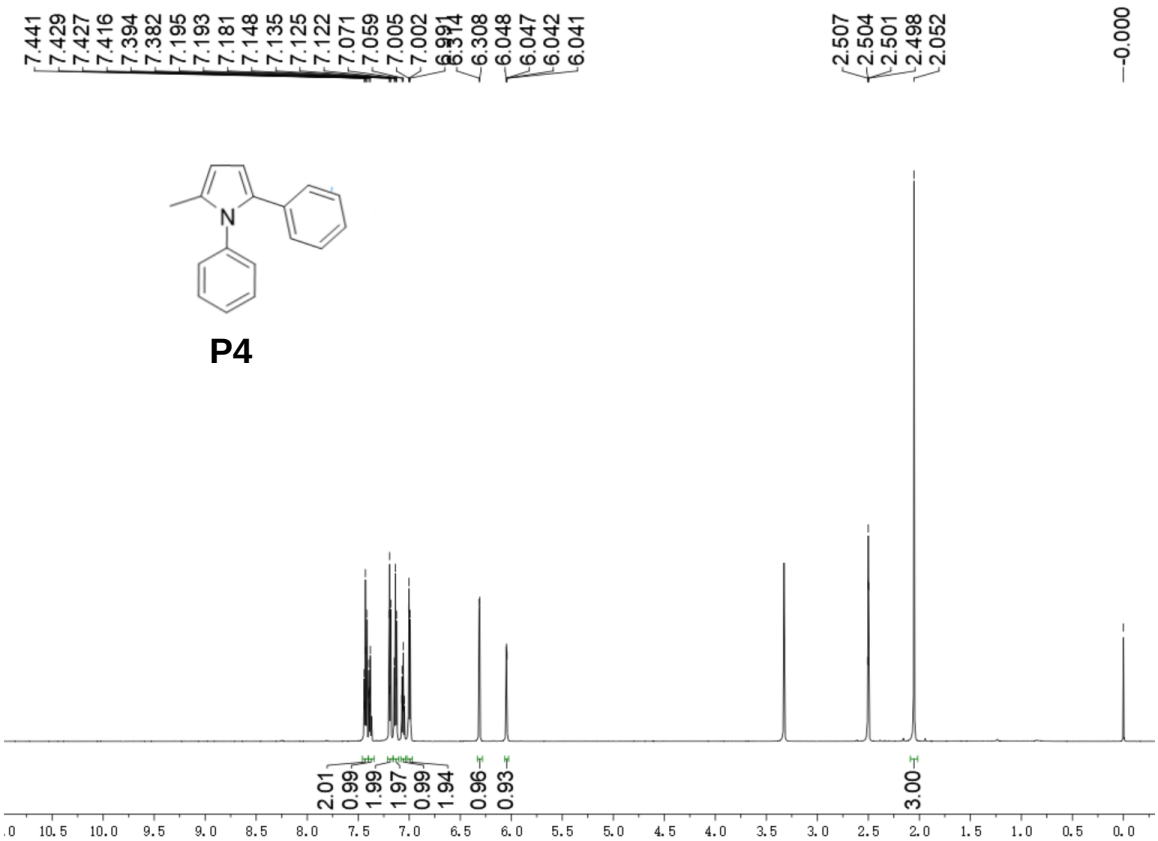


**Figure S3.** $^{1}$H NMR spectrum of **P4** in DMSO-$d_6$.

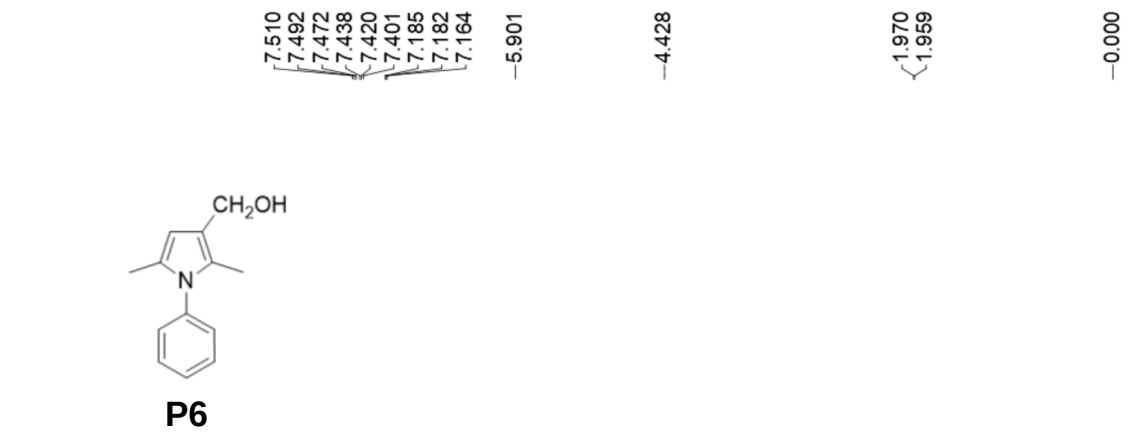


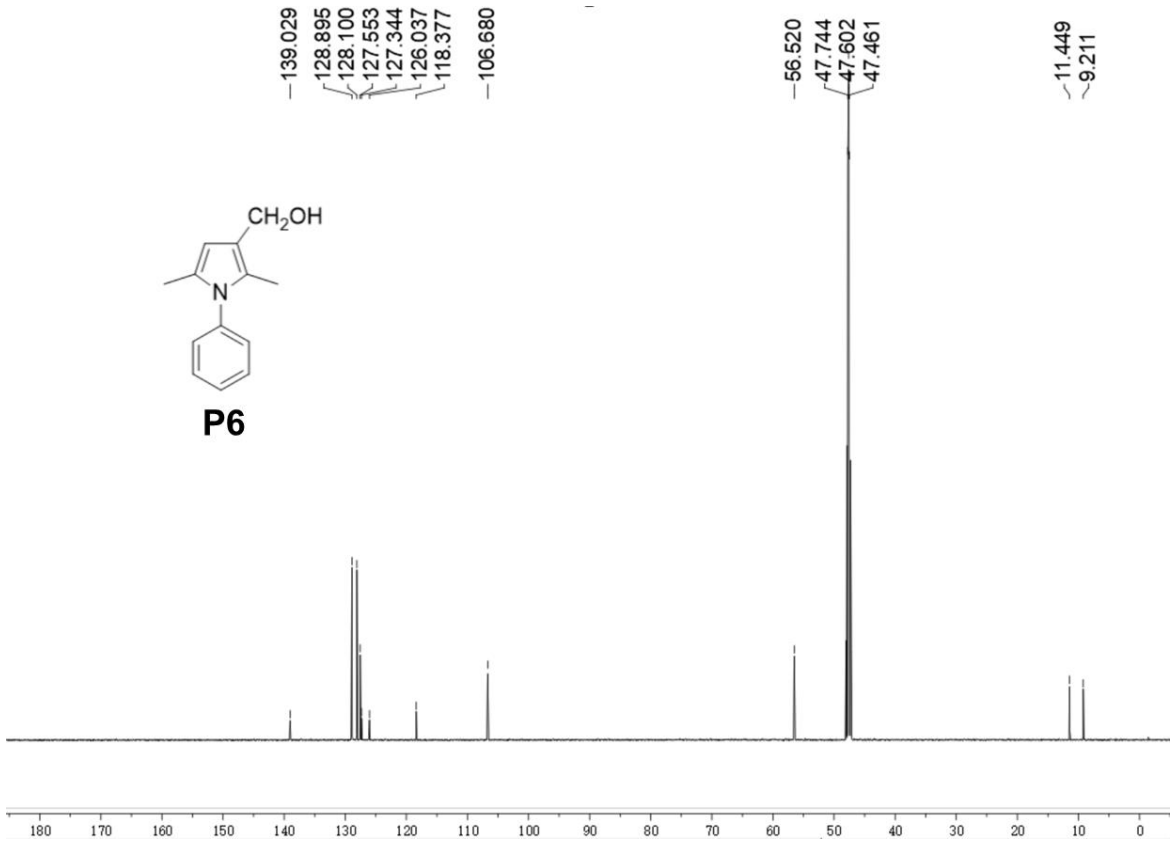


**Figure S4.** $^{1}$H and $^{13}$C NMR spectrum of **P6** in MeOD.

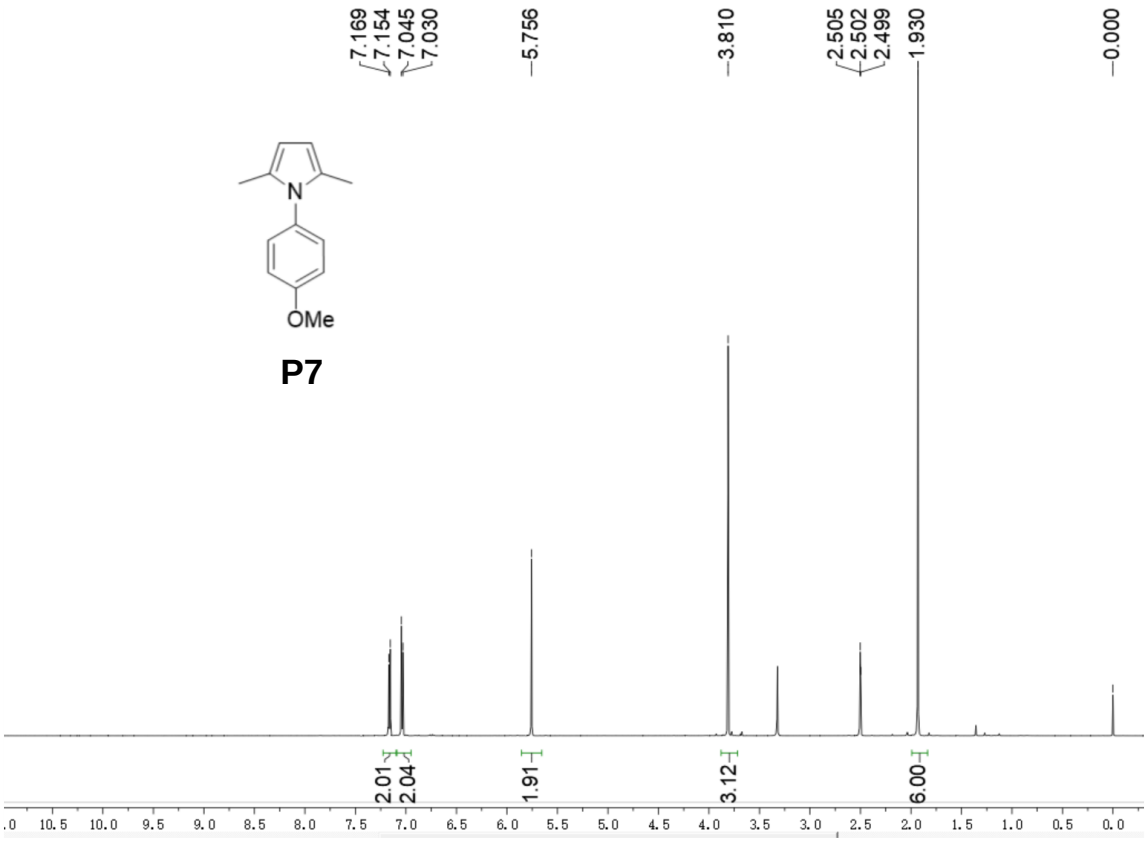


**Figure S5.** $^{1}$H NMR spectrum of **P7** in DMSO-$d_6$.

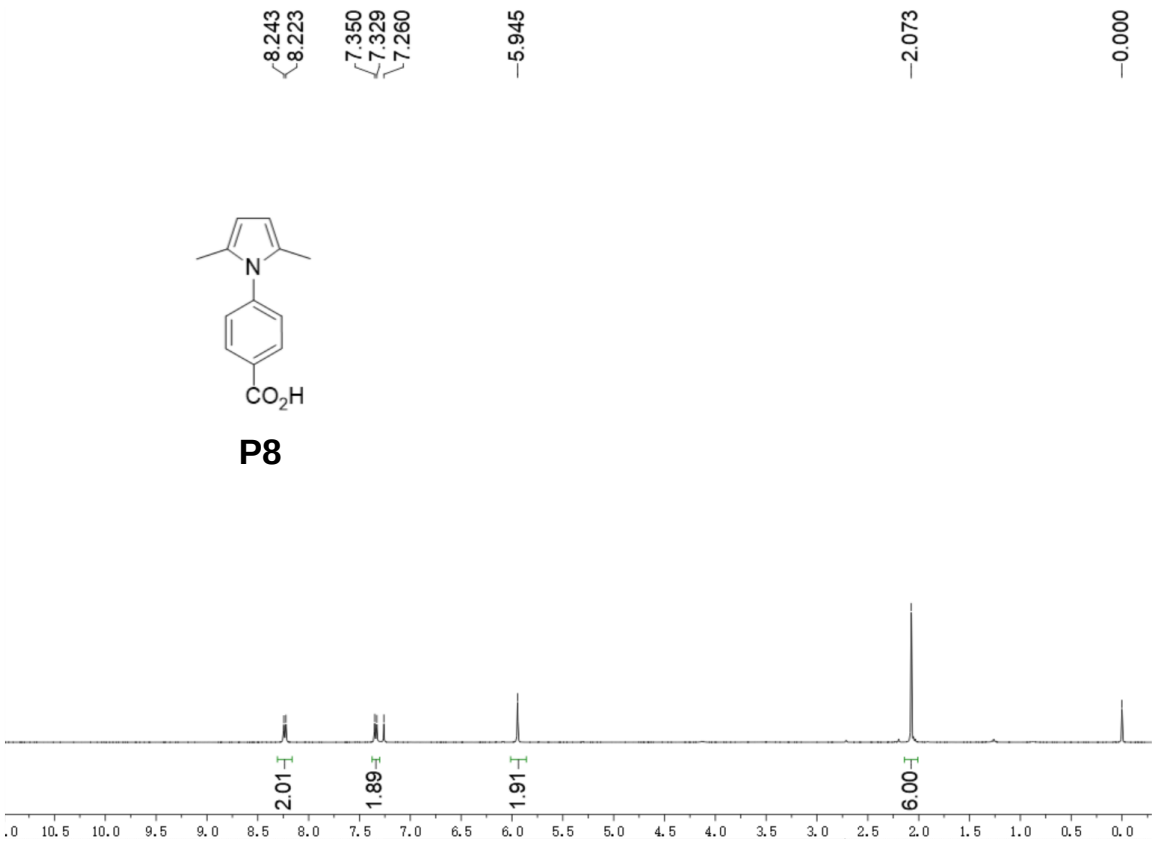


**Figure S**6. $^{1}$H NMR spectrum of **P8** in $CDCl_3$.

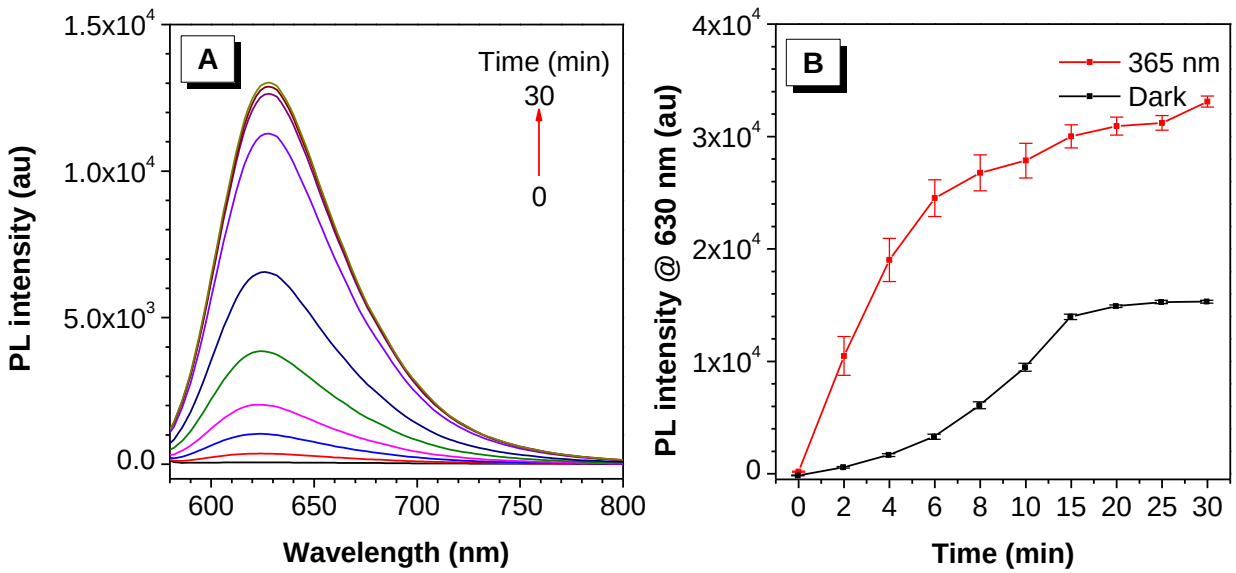


**Figure S7.** (A) PL spectra of **P1**$^{\bullet+}$ on TLC plate under dark and air for 0-30 min, $\lambda_{ex}$ = 550 nm. (B) Plots of PL intensities at 630 nm of **P1**$^{\bullet+}$ on TLC plate under 365 nm light irradiation and dark conditions for 0-30 min, $\lambda_{ex}$ = 600 nm.

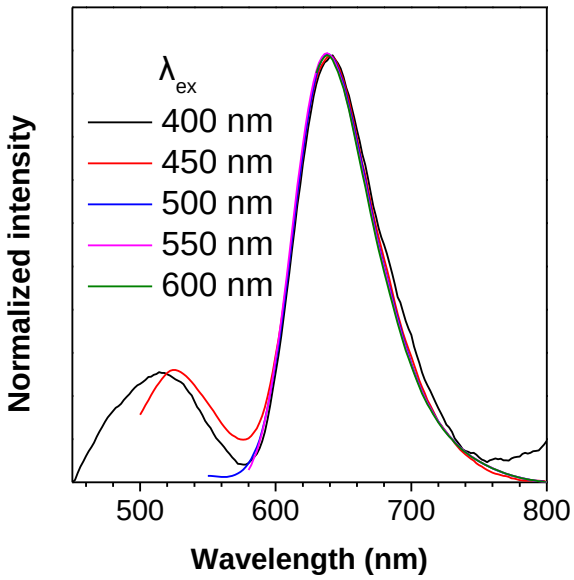


**Figure S8.** Normalized PL spectra of **P1**$^{\bullet+}$ on TLC plate after 365 nm light irradiation for 20 min with different excitation wavelengths of 400 nm, 450 nm, 500 nm, 550 nm and 600 nm.

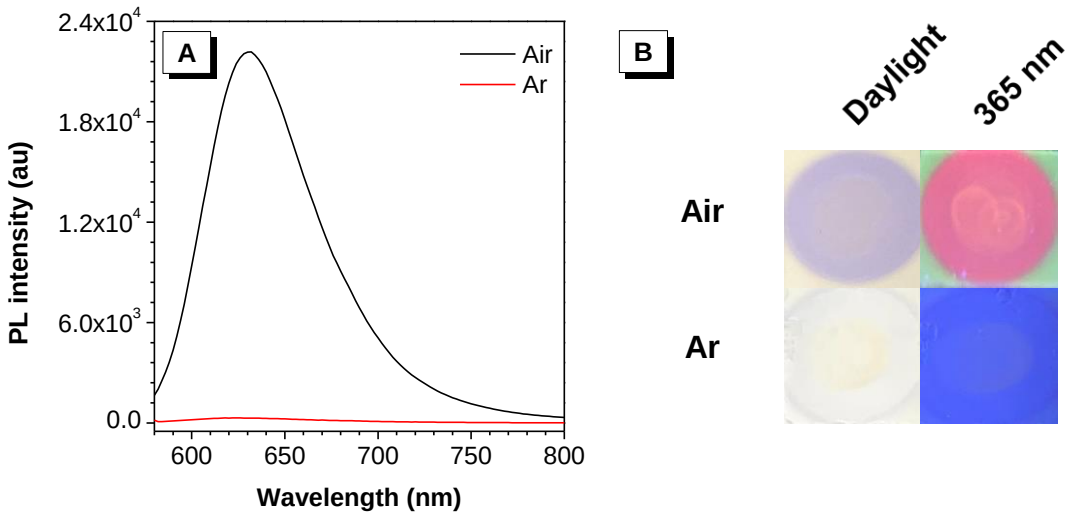


**Figure S9.** (A) PL spectra and (B) Photos of **P1**$^{\bullet+}$ on TLC plate under air and argon after 365 nm light irradiation for 6 min, $\lambda_{ex}$ = 550 nm.

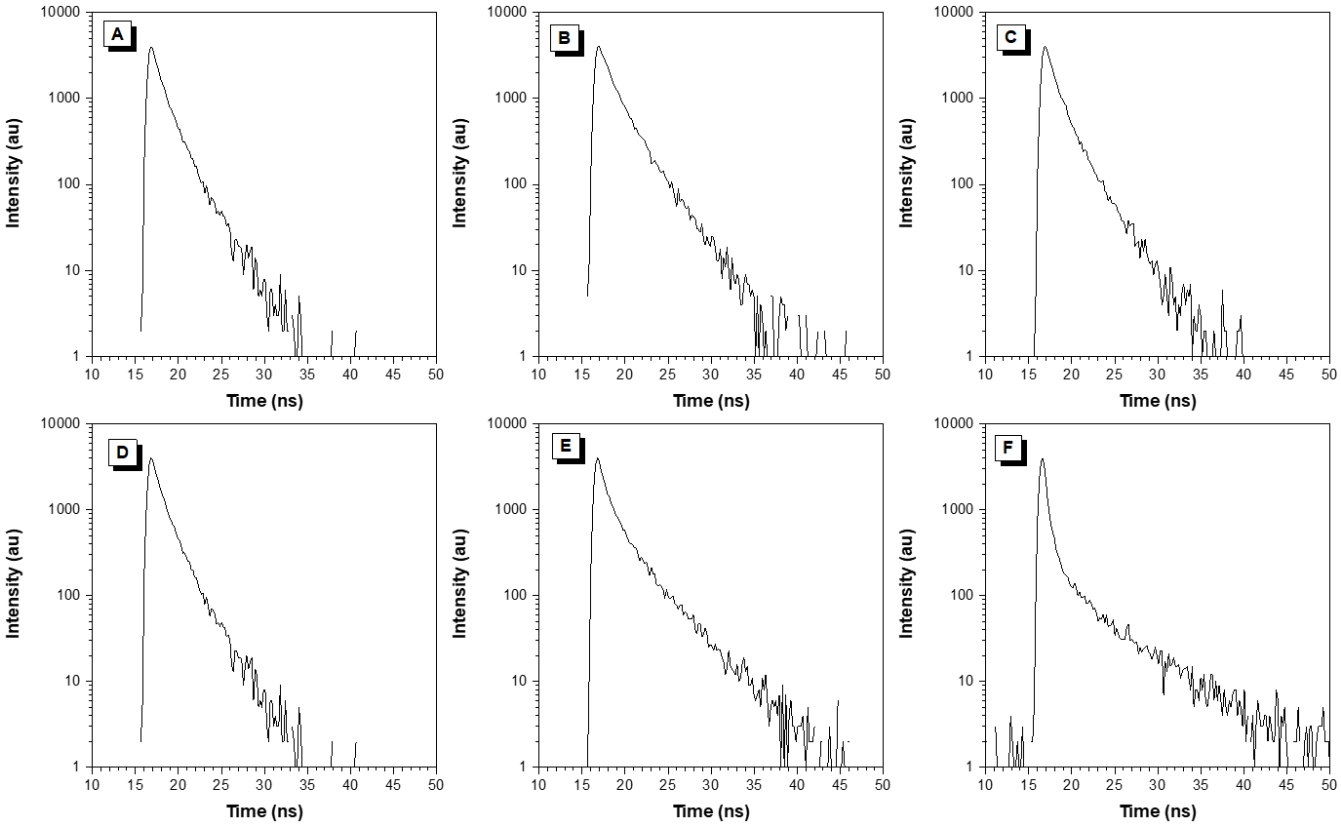


**Figure S10.** Fluorescence lifetime spectra of (A) **P1**$^{\bullet+}$, (B) **P6**$^{\bullet+}$, (C) **P7**$^{\bullet+}$, (D) **P8**$^{\bullet+}$, (E) **P9**$^{\bullet+}$ on TLC plate; (F) **P6**$^{\bullet+}$⊂CB[7] in water (**P6** : CB[7] = 3 : 1, [**P6**] = 10 mM).

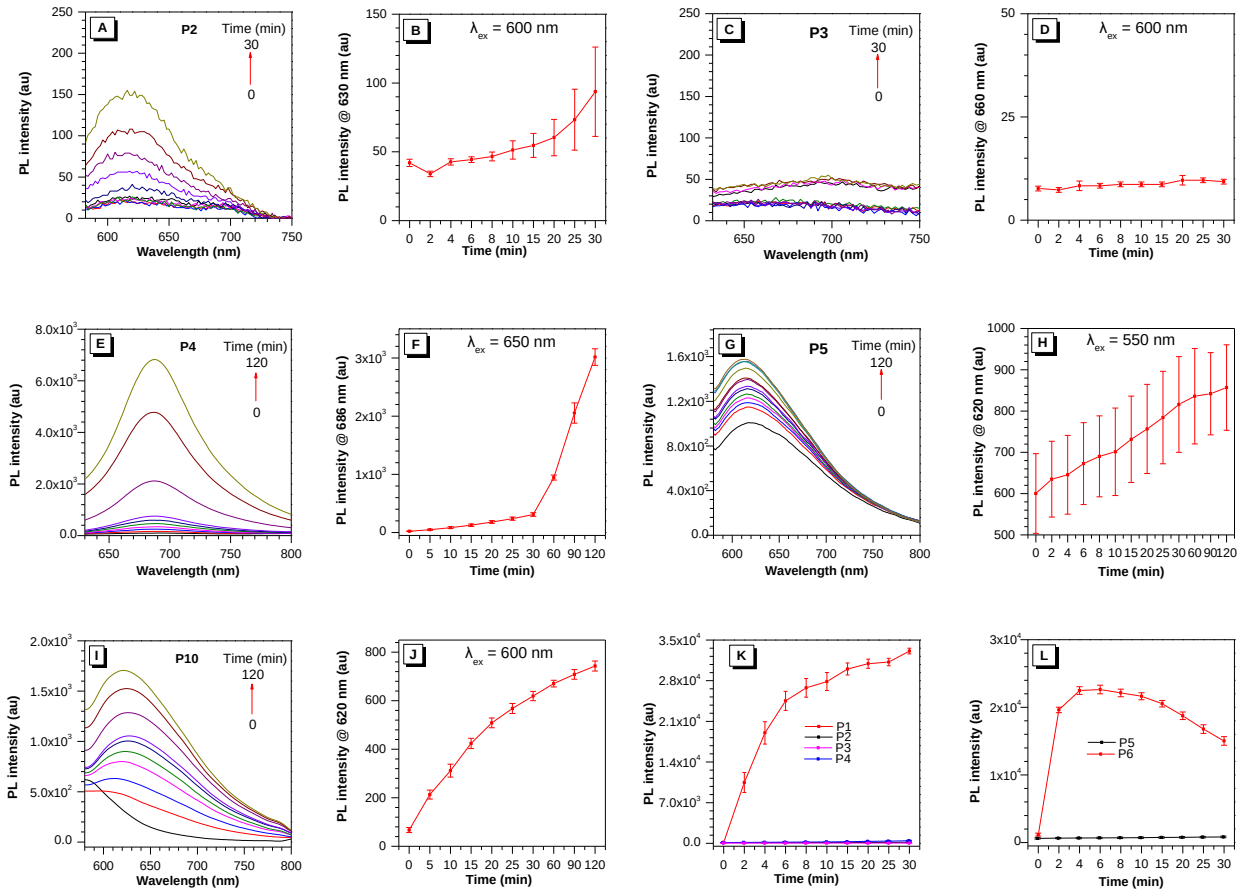


**Figure S11.** (A, G, I) PL spectra of in situ generated **P2**$^{\bullet+}$, **P5**$^{\bullet+}$, **P10**$^{\bullet+}$ on TLC plate under 365 nm light irradiation for different time; $\lambda_{ex}$ = 550 nm; (C) PL spectra of **P3** on TLC plate under 365 nm light irradiation for different time; $\lambda_{ex}$ = 600 nm; (E) PL spectra of in situ generated **P4**$^{\bullet+}$ on TLC plate under 365 nm light irradiation for different time; $\lambda_{ex}$ = 600 nm; (B, D, F, H, J) Plots of PL intensities of **P2**$^{\bullet+}$, **P3**, **P4**$^{\bullet+}$, **P5**$^{\bullet+}$, **P10**$^{\bullet+}$ at 630, 660, 686, 620, 620 nm versus irradiation time, respectively; (K, L) Plots of PL intensities of **P1-P6** on TLC plate under 365 nm light irradiation for different time.

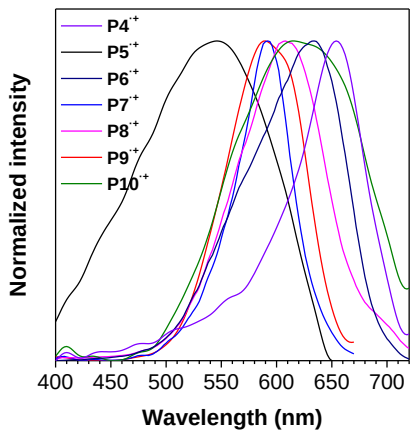


**Figure S12.** Normalized excitation spectra of in situ generated **P4**$^{\bullet+}$, **P5**$^{\bullet+}$, **P6**$^{\bullet+}$, **P7**$^{\bullet+}$, **P8**$^{\bullet+}$, **P9**$^{\bullet+}$ and **P10**$^{\bullet+}$ on TLC plate; for **P4**$^{\bullet+}$, **P6**$^{\bullet+}$, **P8**$^{\bullet+}$ and **P10**$^{\bullet+}$, $\lambda_{em}$ = 750 nm; for **P5**$^{\bullet+}$, $\lambda_{em}$ = 680 nm, for **P7**$^{\bullet+}$ and **P9**$^{\bullet+}$, $\lambda_{em}$ = 700 nm.

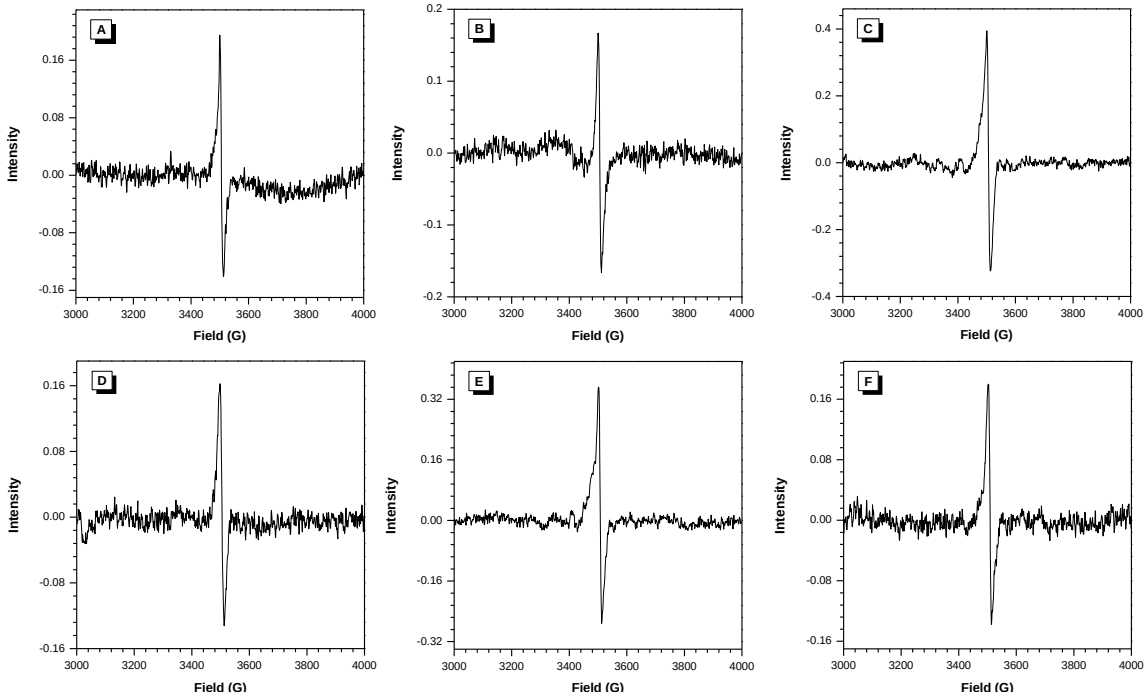


**Figure S13.** EPR spectra of in situ generated (A) **P1**$^{\bullet+}$, (B) **P7**$^{\bullet+}$, (C) **P8**$^{\bullet+}$, (D) **P9**$^{\bullet+}$, (E) **P10**$^{\bullet+}$ on silica gel; (F) EPR spectra of **P6**$^{\bullet+}$⊂CB[7] powder with molar ratio of **P6** : CB[7] = 3 : 1.

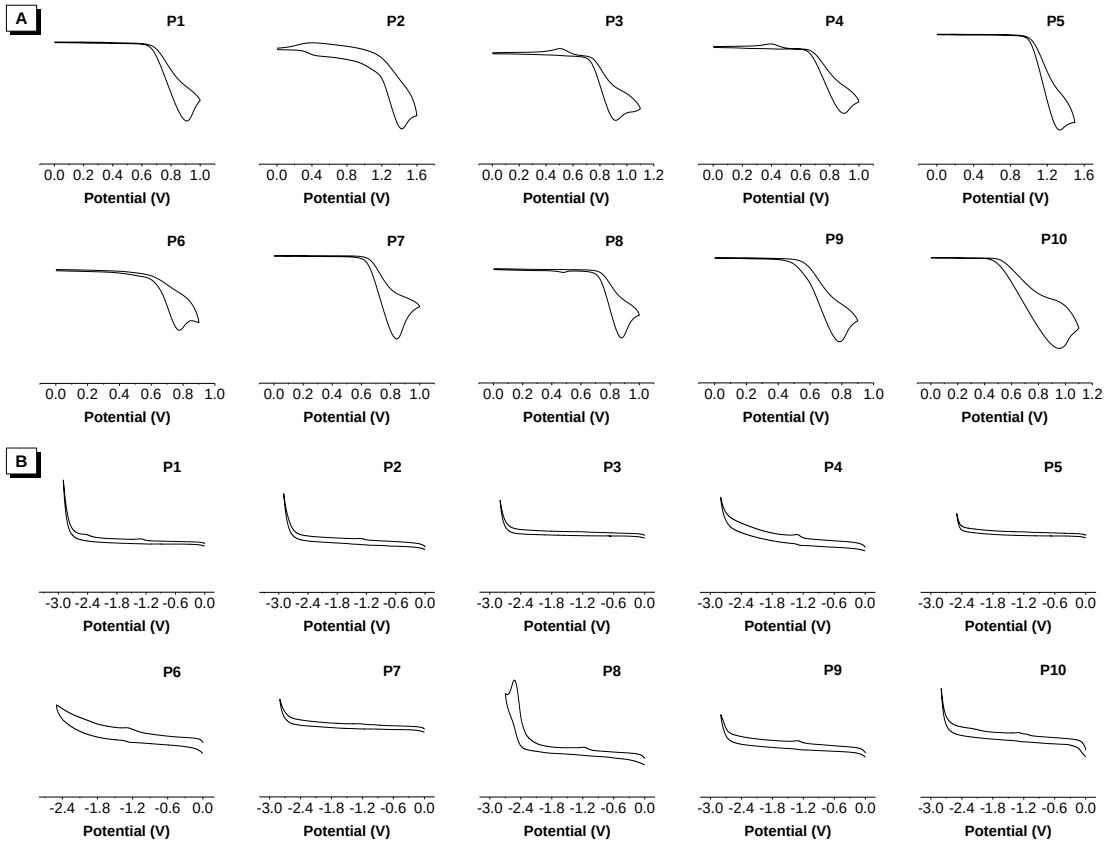


**Figure S14.** (A) Oxidative and (B) reductive cyclic voltammograms of **P1-P10** (1.0 mg mL$^{-1}$) in $CH_2Cl_2$ and DMF containing 0.1 M *n*-$Bu_4NPF_6$, respectively.

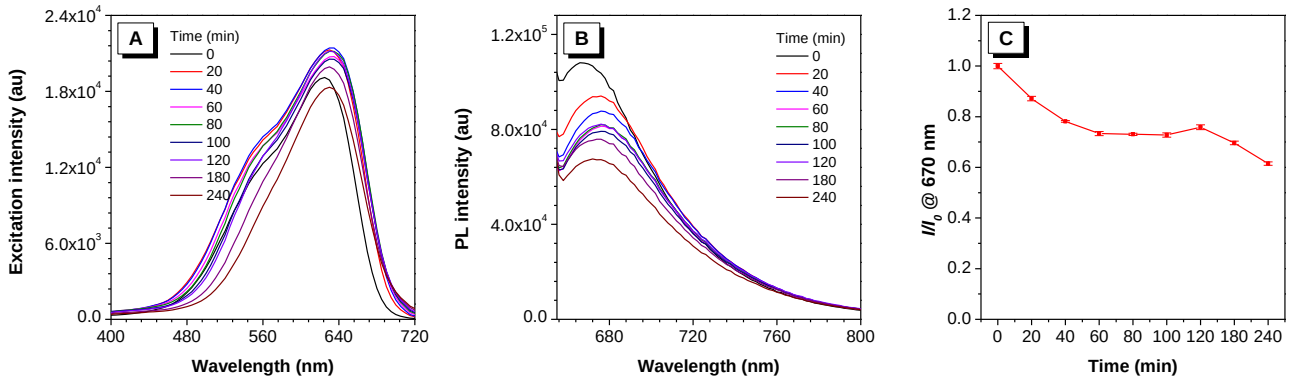


**Figure S15.** Time-dependent (A) excitation spectra of **P6**$^{\bullet+}$ on TLC plate, $\lambda_{em}$ = 750 nm; (B) PL spectra of **P6**$^{\bullet+}$ on TLC plate, $\lambda_{ex}$ = 630 nm; (C) Plots of relative PL intensity ($I/I_0$) at 670 nm of **P6**$^{\bullet+}$ on TLC plate, $\lambda_{ex}$ = 630 nm.

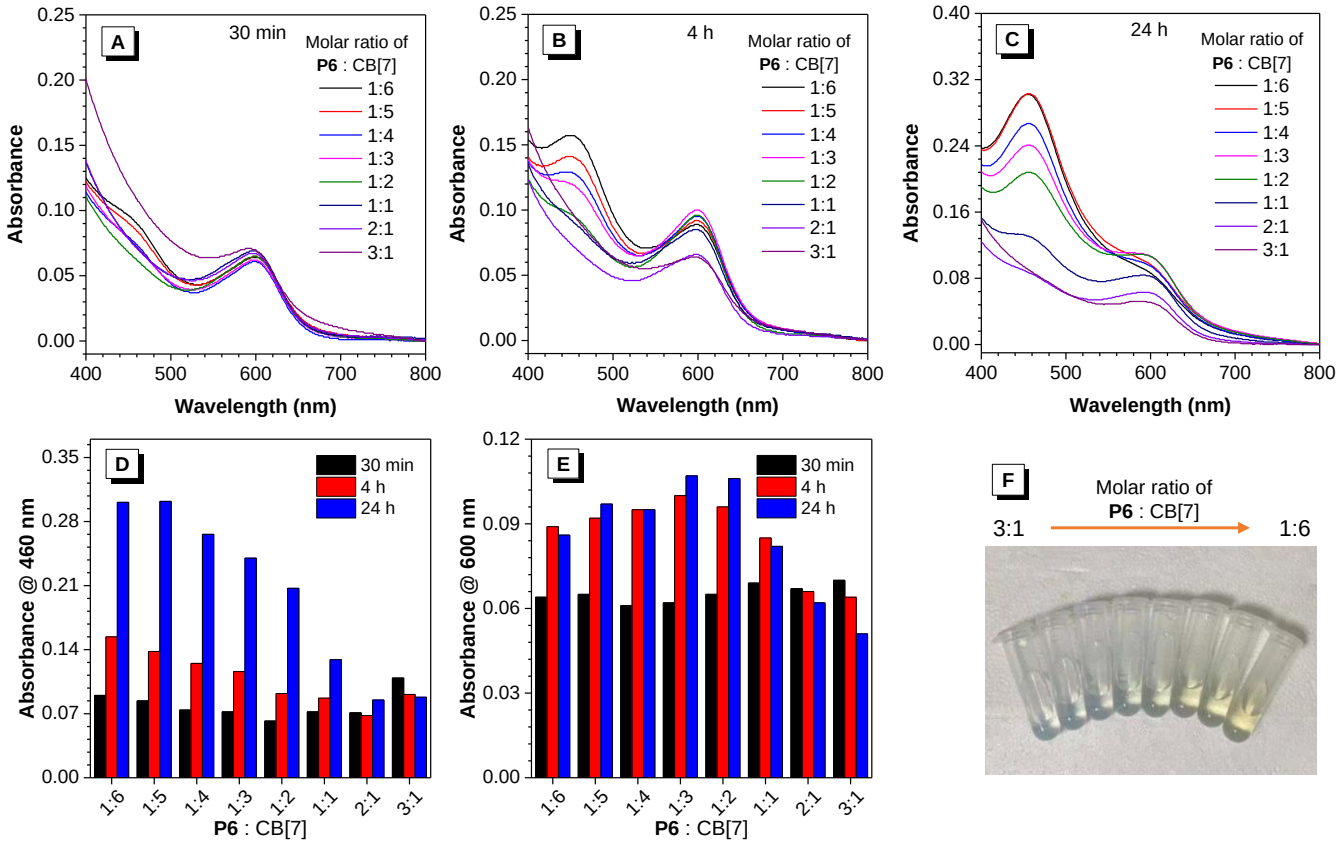


**Figure S16.** UV-Vis absorption spectra of **P6**$^{\bullet+}$⊂CB[7] complex in DMSO/$H_2O$ mixture ($f_w$ = 99%) after mixing of **P6** and CB[7] with different molar ratios for different time: (A) 30 min; (B) 4 h; (C) 24 h; (D, E) Absorbance intensity of **P6**$^{\bullet+}$⊂CB[7] complex at 460 nm and 600 nm versus different molar ratios of **P6**$^{\bullet+}$ : CB[7] after mixing for 30 min, 4 h and 24 h; (F) Photograph of **P6**$^{\bullet+}$⊂CB[7] complex at different molar ratios of **P6**$^{\bullet+}$ : CB[7]. [**P6**] = 300 μM.

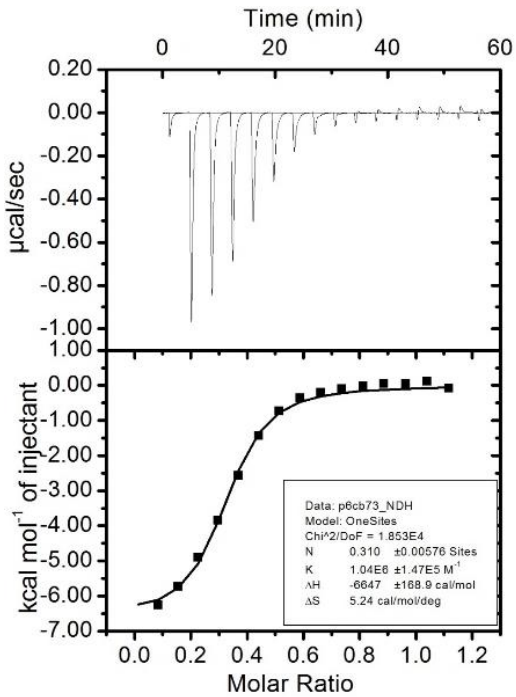


**Figure S17**. The ITC titration data of **P6** (0.05 mM ) treated with a solution of CB[7] (0.5 mM) in the syringe in $H_2O$ at 25 ºC. The binding constant between in situ generated **P6**$^{\bullet+}$ and CB[7] was calculated to be $1.04 \times 10^6$ $M^{-1}$.

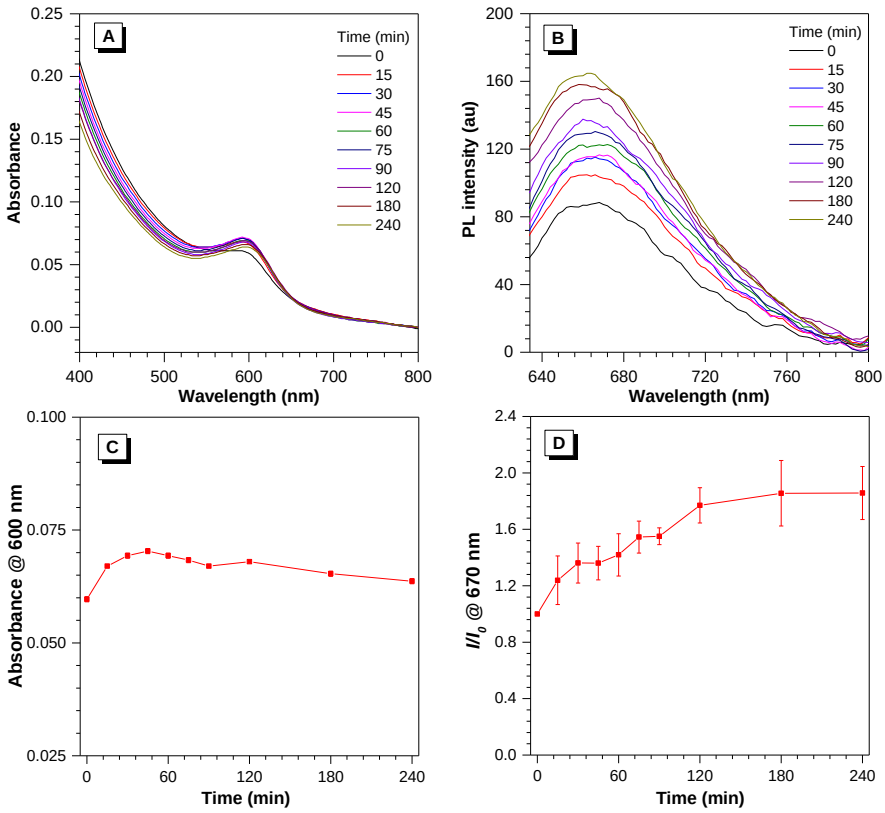


**Figure S18.** (A, B) Time-dependent UV-Vis absorption and PL spectra of **P6**$^{\bullet+}$⊂CB[7] complex in DMSO/$H_2O$ mixture ($f_w$ = 99%); (C, D) Plots of absorbance intensity of **P6**$^{\bullet+}$⊂CB[7] at 600 nm and relative emission intensity ($I/I_0$) at 670 nm versus time; Molar ratio of **P6** : CB[7] = 3 : 1, [**P6**] = 300 µM; $\lambda_{ex}$ = 600 nm.

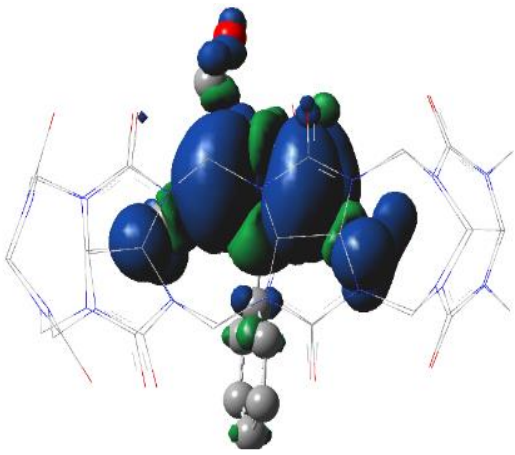

**Figure S19.** Mulliken spin population analysis of **P6**$^{\bullet+}$⊂CB[7]. Blue and green color respectively indicates the spin population of α and β electron. The spin density was drawn at the isovalue of $4\times10^{-4}$ e/bohr$^3$. The spin population of atoms in benzene ring were not shown due to their small absolute values. Hydrogen atoms are omitted for clarity.

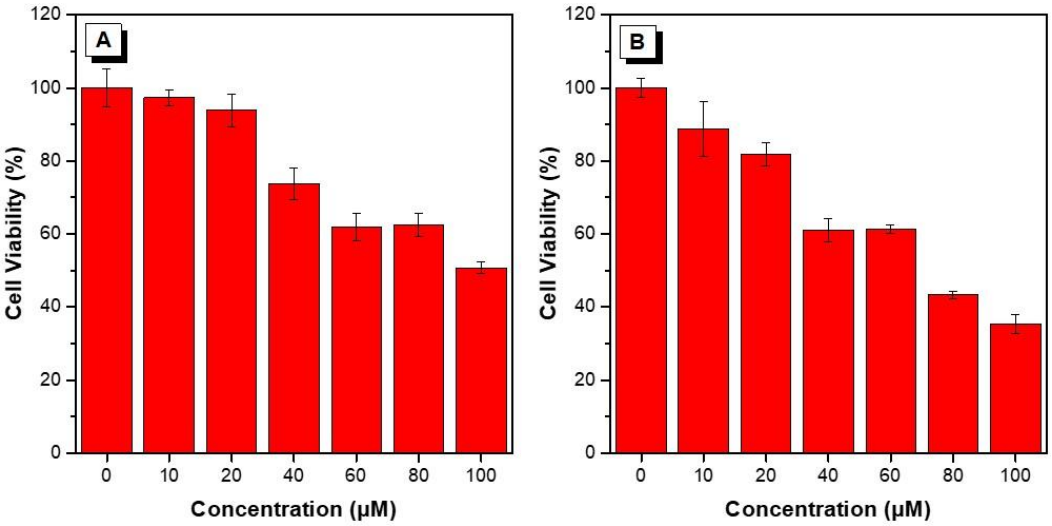


**Figure S20.** Cell viabilities of (A) HeLa cells and (B) A375 cells incubated with **P6**$^{\bullet+}$⊂CB[7] at different concentrations with molar ratio of **P6** : CB[7] = 3:1; ([**P6**] = 0, 10, 20, 40, 60, 80, 100 μM).

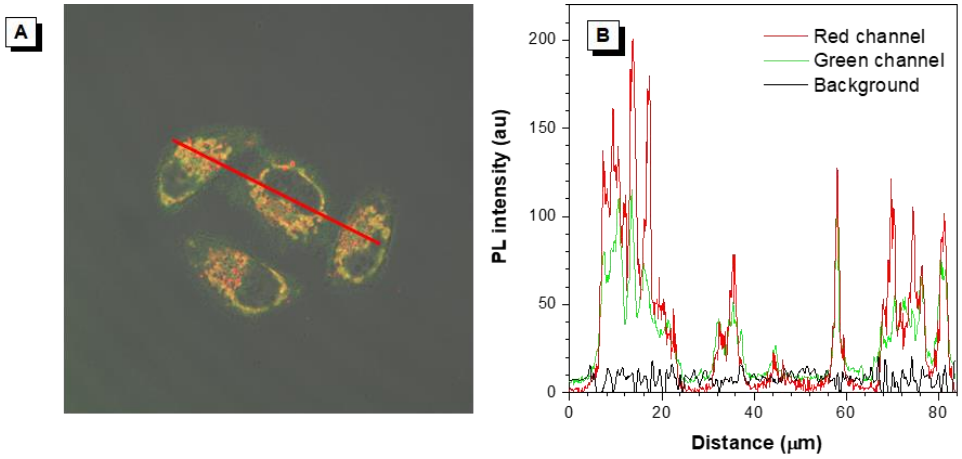


**Figure S21.** (A, B) The cell images and intensity profile of ROI lines. For red channel of **P6**$^{\bullet+}$⊂CB[7], $\lambda_{ex}$ = 633 nm; $\lambda_{em}$ = 640-750 nm; for green channel of MitoTracker Green, $\lambda_{ex}$ = 488 nm; $\lambda_{em}$ = 500-550 nm.

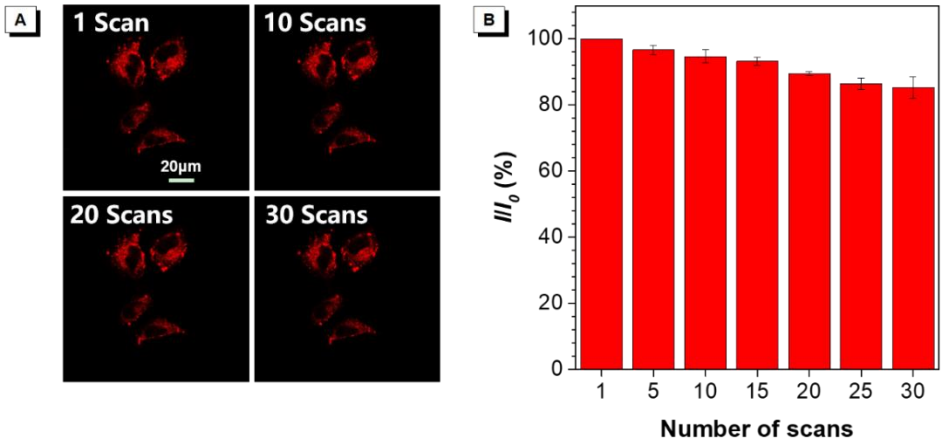


**Figure S22.** Photostability of **P6**$^{\bullet+}$⊂CB[7] in HeLa cells under 633 nm laser irradiation (5% power) for 30 scans.

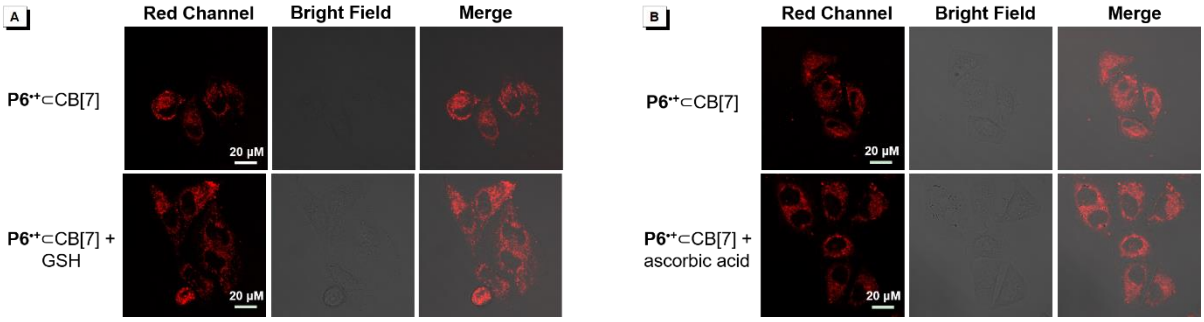


**Figure S23**. (A, B) CLSM images of HeLa cells treated with **P6**$^{\bullet+}$⊂CB[7], "**P6**$^{\bullet+}$⊂CB[7] + GSH" and "**P6**$^{\bullet+}$⊂CB[7] + ascorbic acid". [GSH] = 100 μM; [ascorbic acid] = 50 μM.

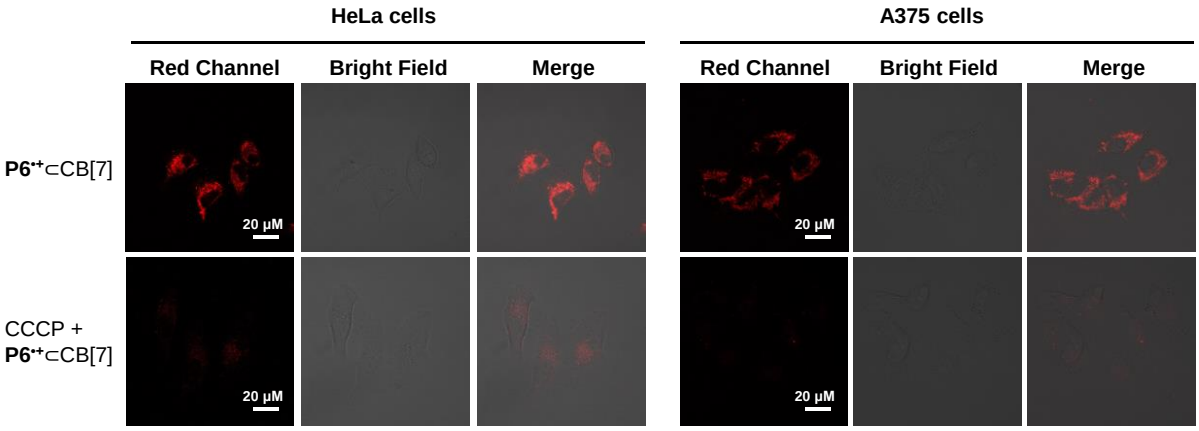


**Figure S24.** CLSM images of HeLa or A375 cells stained with **P6**$^{\bullet+}$⊂CB[7] without and with pre-treatment of CCCP (20 μM).

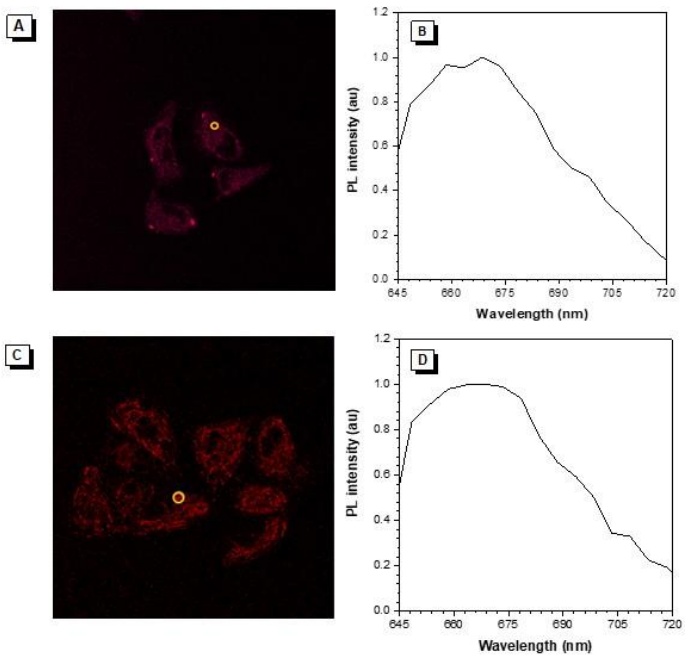


**Figure S25.** Fluorescent images and in situ fluorescence spectra based on Lambda scan mode (indicated by the yellow circles) of live (A, B) HeLa cells and (C, D) A375 cells stained with **P6**$^{\bullet+}$⊂CB[7] for 3 h; Molar ratio of **P6** : CB[7] = 3 : 1, [**P6**] = 20 μM; $\lambda_{ex}$ = 633 nm; $\lambda_{em}$ = 643-723 nm.

## References


1 B. K. Banik, S. Samajdar and I. Banik, *J. Org. Chem.* 2004, **69**, 213-216.

2 M. Biava, G. C. Porretta, G. Poce, A. De Logu, M. Saddi, R. Meleddu, F. Manetti, E. De Rossi and M. Botta, *J. Med. Chem.* 2008, **51**, 3644-3648.

3 F. Neese, *Wiley Interdisciplinary Reviews-Computational Molecular Science* 2012, **2**, 73-78.

4 M. J. Frisch, G. W. Trucks, H. B. Schlegel, G. E. Scuseria, M. A. Robb, J. R. Cheeseman, G. Scalmani, V. Barone, G. A. Petersson, H. Nakatsuji, X. Li, M. Caricato, A. V. Marenich, J. Bloino, B. G. Janesko, R. Gomperts, B. Mennucci, H. P. Hratchian, J. V. Ortiz, A. F. Izmaylov, J. L. Sonnenberg, Williams, F. Ding, F. Lipparini, F. Egidi, J. Goings, B. Peng, A. Petrone, T. Henderson, D. Ranasinghe, V. G. Zakrzewski, J. Gao, N. Rega, G. Zheng, W. Liang, M. Hada, M. Ehara, K. Toyota, R. Fukuda, J. Hasegawa, M. Ishida, T. Nakajima, Y. Honda, O. Kitao, H. Nakai, T. Vreven, K. Throssell, J. A. Montgomery Jr., J. E. Peralta, F. Ogliaro, M. J. Bearpark, J. J. Heyd, E. N. Brothers, K. N. Kudin, V. N. Staroverov, T. A. Keith, R. Kobayashi, J. Normand, K. Raghavachari, A. P. Rendell, J. C. Burant, S. S. Iyengar, J. Tomasi, M. Cossi, J. M. Millam, M. Klene, C. Adamo, R. Cammi, J. W. Ochterski, R. L. Martin, K. Morokuma, O. Farkas, J. B. Foresman and D. J. Fox, Wallingford, CT, **2016**.

5 D. A. Case, K. Belfon, I. Y. Ben-Shalom, S. R. Brozell, D. S. Cerutti, I. T.E. Cheatham, V.W.D. Cruzeiro, T. A. Darden, R. E. Duke, G. Giambasu, M. K. Gilson, H. Gohlke, R. H. A.W. Goetz, S. Izadi, K. Kasavajhala, A. Kovalenko, R. Krasny, T. Kurtzman, T. S. Lee, S. LeGrand, P. Li, C. Lin, J. Liu, T. Luchko, R. Luo, V. Man, K. M. Merz, Y. Miao, O. Mikhailovskii, G. Monard, H. Nguyen, A. Onufriev, F. Pan, S. Pantano, R. Qi, D. R. Roe, A. Roitberg, C. Sagui, S. Schott-Verdugo, J. Shen, C. L. Simmerling, N. Skrynnikov, J. Smith, J. Swails, R. C. Walker, J. Wang, L. Wilson, R. M. Wolf, X. Wu, D. M. York and P. A. University of California: San Francisco, **2020**.

6 A. T. Fenley, N. M. Henriksen, H. S. Muddana and M. K. Gilson Bridging Calorimetry and Simulation through Precise Calculations of Cucurbituril–Guest Binding Enthalpies. *J. Chem. Theory Comput.* 2014, **10**, 4069-4078.

7 R. Dennington, T. A. Keith and J. M. Millam, Semichem Inc.: Shawnee Mission, KS, **2016**.